

# Inclusive $B$ -Meson Production at the LHC in the GM-VFN Scheme

B. A. Kniehl<sup>1</sup>, G. Kramer<sup>1</sup>, I. Schienbein<sup>2</sup> and H. Spiesberger<sup>3</sup>

<sup>1</sup> II. Institut für Theoretische Physik, Universität Hamburg,  
Luruper Chaussee 149, D-22761 Hamburg, Germany

<sup>2</sup> Laboratoire de Physique Subatomique et de Cosmologie,  
Université Joseph Fourier Grenoble 1,  
CNRS/IN2P3, Institut National Polytechnique de Grenoble,  
53 avenue des Martyrs, F-38026 Grenoble, France

<sup>3</sup> Institut für Physik, Johannes-Gutenberg-Universität,  
Staudinger Weg 7, D-55099 Mainz, Germany

## Abstract

We calculate the next-to-leading-order cross section for the inclusive production of  $B$  mesons in  $pp$  collisions in the general-mass variable-flavor-number scheme, an approach which takes into account the finite mass of the  $b$  quarks. We use realistic evolved nonperturbative fragmentation functions obtained from fits to  $e^+e^-$  data and compare our results for the transverse-momentum and rapidity distributions at a center-of-mass energy of 7 TeV with recent data from the CMS Collaboration at the CERN LHC. We find good agreement, in particular at large values of  $p_T$ .

PACS: 12.38.Bx, 12.39.St, 13.85.Ni, 14.40.Nd

# 1 Introduction

Since the late eighties there has been much interest in the study of  $B$ -meson production in  $p\bar{p}$  and  $pp$  collisions at hadron colliders, both experimentally and theoretically. The first measurements were performed more than two decades ago by the UA1 Collaboration at the CERN  $S\bar{p}pS$  collider [1] operating at a center-of-mass energy of  $\sqrt{S} = 0.63$  TeV. More recent measurements were made by the CDF and D0 Collaborations at the Fermilab Tevatron running at  $\sqrt{S} = 1.8$  TeV [2, 3] and 1.96 TeV [4]. Just recently, the CMS Collaboration at the CERN LHC collider published first results for inclusive  $B^+$ - [5],  $B^0$ - [6], and  $B_s$ -meson [7] production in  $pp$  collisions at  $\sqrt{S} = 7$  TeV.  $B^+$  mesons were reconstructed via their decay  $B^+ \rightarrow J/\psi K^+$  followed by  $J/\psi \rightarrow \mu^+\mu^-$ , whereas  $B^0$  mesons were identified through the observation of  $J/\psi K_s^0$  final states with the subsequent decays  $J/\psi \rightarrow \mu^+\mu^-$  and  $K_s^0 \rightarrow \pi^+\pi^-$ . In the case of  $B_s$  mesons, the reconstructed final states were generated by the decay chain  $B_s \rightarrow J/\psi\phi$ ,  $J/\psi \rightarrow \mu^+\mu^-$ , and  $\phi \rightarrow K^+K^-$ . From all these measurements the differential cross sections  $d\sigma/dp_T$  and  $d\sigma/dy$  as well as the integrated cross section for  $p_T \geq 5$  GeV (for  $B^+$  and  $B^0$  mesons) or  $p_T \geq 8$  GeV (for  $B_s$  mesons) were reported.

The general-mass variable-flavor-number (GM-VFN) scheme provides a rigorous theoretical framework for the description of the inclusive production of single heavy-flavored hadrons, combining the fixed-flavor-number (FFN) [8] and zero-mass variable-flavor-number (ZM-VFN) [9] schemes, which are valid in complementary kinematic regions, in a unified approach that enjoys the virtues of both schemes and, at the same time, is bare of their flaws. Specifically, it resums large logarithms by the Dokshitzer-Gribov-Lipatov-Altarelli-Parisi (DGLAP) evolution of nonperturbative fragmentation functions (FFs), guarantees the universality of the latter as in the ZM-VFN scheme, and simultaneously retains the mass-dependent terms of the FFN scheme without additional theoretical assumptions. It was elaborated at next-to-leading order (NLO) for photoproduction [10] and hadroproduction [11] of charmed hadrons as well as for their production by  $e^+e^-$  annihilation [12]. It was also applied to obtain predictions for  $B$ -meson hadroproduction [13], which could be compared with recent CDF data [4]. An earlier implementation of such an interpolating scheme is the so-called fixed-order-next-to-leading-logarithm (FONLL) approach, in which the conventional cross section in the FFN scheme is linearly combined, with the help of a  $p_T$ -dependent weight function, with a suitably modified cross section in the ZM-VFN scheme implemented with perturbative FFs [14].

In Ref. [13], nonperturbative FFs for the transitions  $a \rightarrow B$ , where  $a$  is any parton, including  $b$  and  $\bar{b}$  quarks, were extracted at NLO in the  $\overline{\text{MS}}$  factorization scheme with  $n_f = 5$  flavors from the scaled-energy ( $x$ ) distributions  $d\sigma/dx$  of  $e^+e^- \rightarrow B + X$  measured by the ALEPH [15] and OPAL [16] Collaborations at the CERN LEP1 collider and by the SLD Collaboration [17] at the SLAC SLC collider. As explained in Ref. [13], these FFs may be consistently used in our GM-VFN framework. Working at NLO in the GM-VFN scheme with these  $B$ -meson FFs, we found excellent agreement with recent CDF measurements of  $d\sigma/dp_T$  for  $p\bar{p} \rightarrow B + X$  [4], especially in the upper  $p_T$  range,  $p_T \gtrsim 10$

GeV [13].

The content of this paper is as follows. In Sec. 2, we summarize our input choices of PDFs and  $B$ -meson FFs. In Sec. 3, we compare the predictions of the GM-VFN scheme with the CMS data from the recent LHC run at  $\sqrt{S} = 7$  TeV [5, 6, 7]. Our conclusions are given in Sec. 4.

## 2 Input PDFs and $B$ -meson FFs

As PDFs for the proton, we choose one of the most recent parametrizations of the CTEQ Collaboration, set CTEQ6.6M [18], which provides an improvement over the earlier version CTEQ6.5M. Both sets were obtained in the framework of a general-mass scheme using the input values  $m_c = 1.3$  GeV,  $m_b = 4.5$  GeV, and  $\alpha_s(m_Z) = 0.118$ . In both set, the  $b$ -quark PDF has its starting scale at  $\mu_0 = m_b$ .

The nonperturbative FFs describing the transition of the  $b$  and  $\bar{b}$  quarks into a  $B$  meson can be obtained only from experiment. In our earlier work on inclusive  $B$ -meson production at the Tevatron [13], we constructed such FFs using as input recent precise measurements of the cross section of inclusive  $B$ -meson production in  $e^+e^-$  annihilation obtained by the ALEPH [15], OPAL [16], and SLD [17] Collaborations.<sup>1</sup> These data were taken on the  $Z$ -boson resonance, so that finite- $m_b$  effects, being of relative order  $m_b^2/m_Z^2$ , are strongly suppressed, which means that we are in the asymptotic regime where the GM-VFN scheme is equivalent to the ZM-VFN scheme. The combined fit to the three data sets was performed using the NLO value  $\Lambda_{\overline{MS}}^{(5)} = 227$  MeV corresponding to  $\alpha_s^{(5)}(m_Z) = 0.1181$ , values adopted from Ref. [18]. The renormalization and factorization scales were chosen to be  $\mu_R = \mu_F = m_Z$ . In accordance with the chosen PDFs, the starting scale of the  $b \rightarrow B$  FF was taken to be  $\mu_0 = m_b$ , while the  $g, q \rightarrow B$  FFs, where  $q$  denotes the light quarks including the charm quark, were taken to vanish at  $\mu_F = \mu_0$ .

For fitting the data, we actually employed two different parametrizations for the  $b \rightarrow B$  FF at  $\mu_0 = m_b$ , namely the Peterson ansatz [20] and the simple power ansatz [21]. It turned out that the Peterson ansatz led to a very poor fit. Therefore, we shall use in this work only the FFs obtained with the power ansatz, whose parameters at the starting scale are listed in Table 1 of Ref. [13]. A comparison of the fit performed using this ansatz with the three input data sets may be found in Fig. 1 of that reference.

We note that the data from OPAL and SLD included all  $B$ -hadron final states, in particular those with  $\Lambda_b$  hadrons, while, in the ALEPH analysis, only final states with identified  $B^\pm$  and  $B^0$  mesons were taken into account. Our fit was based on the assumption that the FFs of all  $b$  hadrons had the same shape. The branching fraction of  $b \rightarrow B^+$  was taken equal to that of  $b \rightarrow B^0$  and fixed to 0.397. In our calculations for  $B_s$ -meson production to be presented below, we shall use the same FFs and rescale them by the factor

---

<sup>1</sup> Recently, similar data became available also from the DELPHI Collaboration [19].

0.113/0.401, which uses the up-to-date values for the  $b \rightarrow B^+$  and  $b \rightarrow B_s$  branching fractions quoted by the Particle Data Group [22].

We should emphasize that, in the analysis of the available  $e^+e^-$  annihilation data, the charged and neutral  $B$  mesons were not separated. Furthermore, the charged states  $B^+$  and  $B^-$  could not be distinguished. The FFs obtained in Ref. [13] are, therefore, valid for the average of  $B^+$  and  $B^-$  and, similarly, for the average of  $B^0$  and  $\bar{B}^0$ .

The factorization scales related to the initial- and final-state singularities entering the PDFs and FFs, respectively, can in principle be chosen independently. We checked, however, that when estimating theoretical error bands by varying these scales by factors of 2 up and down, the extreme values are indeed obtained when the initial- and final-state factorization scales are identified. Our default choice of renormalization and factorization scales is  $\mu_R = \mu_F = m_T = \sqrt{p_T^2 + m_b^2}$ . Theoretical uncertainties will be estimated by setting  $\mu_R = \xi_R m_T$  and  $\mu_F = \xi_F m_T$ , and varying  $\xi_R$  and  $\xi_F$  about their default values  $\xi_R = \xi_F = 1$  by factors of 2 up and down, restricting the ratio to the range  $1/2 \leq \xi_R/\xi_F \leq 2$ .

### 3 Theoretical Predictions for $pp \rightarrow B + X$ and Comparisons with CMS Data

To obtain an overview of the  $p_T$  dependence of  $d\sigma/dp_T$ , we first show results for this observable, integrated over  $|y| \leq 2.4$ , for the case of  $B^+$  production in the GM-VFN scheme as described above. This differential cross section is shown in Fig. 1 (left) for  $p_T$  values between 5 and 30 GeV and in Fig. 1 (right) for larger  $p_T$  values, up to 100 GeV, where we expect data to come in the near future when the LHC experiments are accumulating more statistics.

In the  $p_T$  range between 5 and 30 GeV, the cross section falls off by three orders of magnitude. This is essentially due to the behavior of the PDFs as a function of the scaling variable  $x$  and less so from the behavior of the partonic cross sections. Towards low  $p_T$  values, both the upper edge of the error band and the cross section for the default choice of scales rise steadily with decreasing  $p_T$  value, down to  $p_T = 5$  GeV. This is caused by the scale dependence of the  $b$ -quark PDF and the FFs. With our choice of scales, they fade out and quench the cross section, leading to a turn-over of the  $p_T$  distributions only at  $p_T = 0$  and not already at some finite  $p_T$  value. The lower edge of the error band is obtained for  $\xi_F = 0.5$ . Here, both the  $b$ -quark PDF and the FFs vanish at  $p_T \approx 8$  GeV, corresponding to  $\mu_F = m_b = 4.5$  GeV. The line representing the lower edge of the error band therefore stops at this point.

The CMS Collaboration measured the differential cross section  $d\sigma/dp_T$  for the production of  $B^+$  mesons [5] (actually the average of  $B^+$  and  $B^-$  mesons), integrated over the  $y$  range  $|y| \leq 2.4$ , as a function of  $p_T$ . The measurement covered the  $p_T$  range from 5 GeV to

30 GeV with five bins. In addition, the differential cross section  $d\sigma/d|y|$ , integrated over the considered  $p_T$  range, was given for six  $|y|$  bins. In Ref. [6], the results of the measurement of  $B^0$ -meson production (again for the average of the charge-conjugate states  $B^0$  and  $\bar{B}^0$ ) were presented. They comprise the differential cross section  $d\sigma/dp_T$ , integrated over the  $y$  range  $|y| \leq 2.2$ , in five  $p_T$  bins between  $p_T = 5$  GeV and  $p_T = 40$  GeV and  $d\sigma/d|y|$ , integrated over the considered  $p_T$  range, in five  $|y|$  bins. Since, in this second analysis, a larger luminosity was already available, the  $B^0$  data extend to larger  $p_T$  values.

In order to facilitate the comparisons with the CMS measurements [5, 6], we integrate over the bins using the same binnings. The  $p_T$  bins for  $B^{+-}$  and  $B^0$ -meson production are the same, except for the largest one. Our results are shown in Figs. 2 and 3, where they are compared with the experimental data. The errors of the experimental data points are obtained from Ref. [6] by adding in quadrature the statistic and systematic errors quoted there. The differences between the predictions in Figs. 2 and 3 are entirely due to the different bin choices, the FFs being the same in both cases.

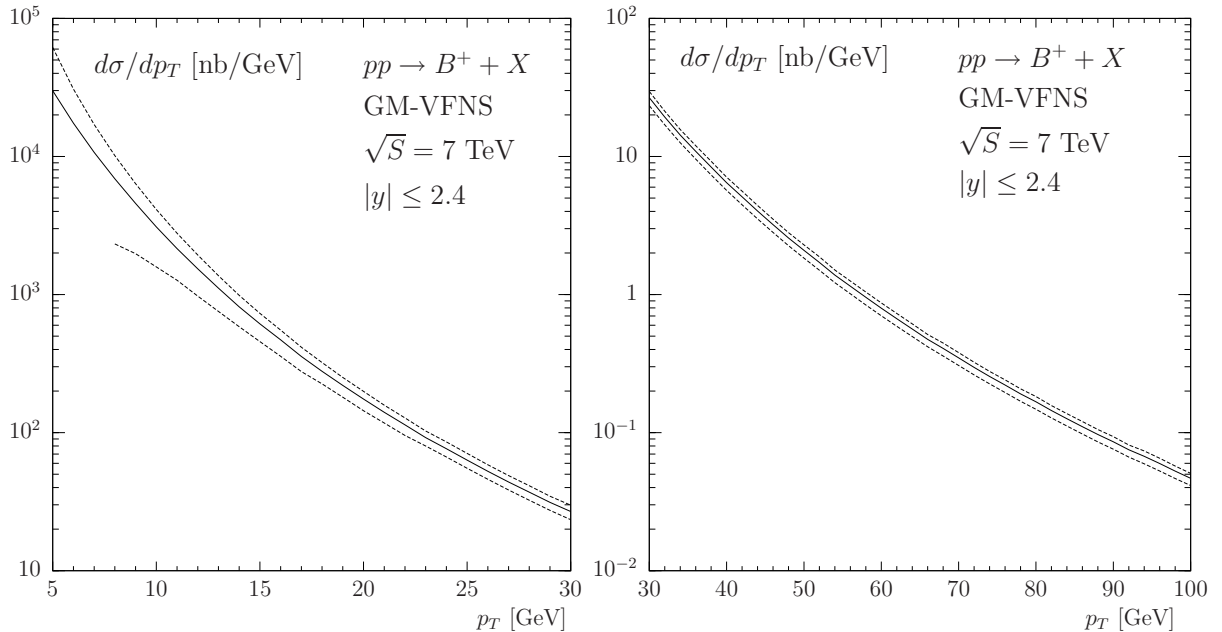


Figure 1:  $d\sigma/dp_T$  [nb/GeV] for  $pp \rightarrow B^+ + X$  at  $\sqrt{S} = 7$  TeV in the GM-VFNS. For clarity, we split the  $p_T$  range into a lower part ( $p_T$  below 30 GeV, left panel) and an upper part ( $p_T$  above 30 GeV, right panel). The central values (solid lines) correspond to the default choice of scale parameters,  $\xi_R = \xi_F = 1$ . An error band (dashed lines) is obtained from variations of the renormalization and factorization scales by factors of 2 up and down. The upper end of the error band is reached for  $\xi_R = 1$  and  $\xi_F = 2$  at  $p_T < 21$  GeV and for  $\xi_R = 0.5$  and  $\xi_F = 1$  at  $p_T > 21$  GeV, the lower error end is reached for  $\xi_R = 1$  and  $\xi_F = 0.5$  at  $p_T < 25$  GeV and  $\xi_R = 2$  and  $\xi_F = 1$  at  $p_T > 25$  GeV.

We determine the error band from variations of the scale parameters by factors of 2 as described above, except that the minimum of the theoretical prediction is obtained with the additional prescription that the FFs are frozen when  $\mu_F$  falls below the starting scale  $\mu_0 = m_b$ . Otherwise the cross section would become zero for  $\xi_F = 0.5$  in a large part of the first  $p_T$  bin, so that the lower edge of the error band would become meaningless. As is seen in Figs. 2 and 3, the data lie inside the error bands. In the case of  $B^+$  ( $B^0$ ) mesons, the default predictions appreciably overshoot the CMS data in the first three (two)  $p_T$  bins, while they are very close to the CMS data in the residual  $p_T$  bins. The default values of the predicted cross sections are a factor of approximately 2 (1.5) larger than the experimental central values in the lowest (next-to-lowest)  $p_T$  bins. This is caused by the fact that, with our choice of scales, large contributions coming from initial-state  $b$  quarks are present for all finite values of  $p_T$ . If one changes the factorization scale to a lower value, for example by setting  $\xi_R = 1$  and  $\xi_F = 0.7$ , the  $b$ -quark PDF vanishes at  $p_T = 4.6$  GeV. Furthermore, with our prescription, the PDFs and the FFs are frozen at the values they reach at  $\mu_F = m_b$  when  $p_T$  falls below  $p_T = 4.6$  GeV. For this special choice of factorization scales, we obtain the cross section values given for the  $B^0$ -meson case in the column labeled  $\xi_R = 1$ ,  $\xi_F = 0.7$  of Tab. 1. For comparison, we present the

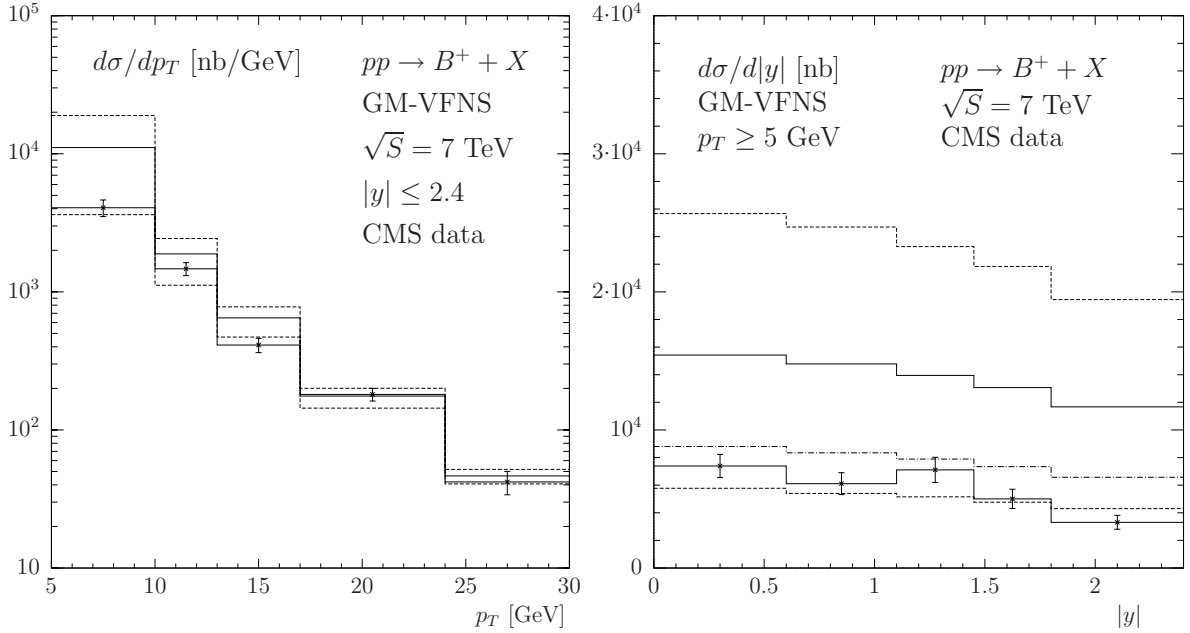


Figure 2:  $d\sigma/dp_T$  [nb/GeV] (left panel) and  $d\sigma/d|y|$  [nb] (right panel) for  $pp \rightarrow B^+ + X$  at NLO in the GM-VFN scheme compared with the CMS data [5]. The central values (solid lines) correspond to the choice  $\xi_R = \xi_F = 1$ . We also show the prediction for  $d\sigma/d|y|$  obtained with the choice  $\xi_R = 1$  and  $\xi_F = 0.7$  (dash-dotted line). The error bands (dashed lines) are obtained by varying  $\xi_R$  and  $\xi_F$  by factors of 2 up and down (maximum:  $\xi_R = 1$ ,  $\xi_F = 2$ ; minimum:  $\xi_R = 1$ ,  $\xi_F = 0.5$ ).

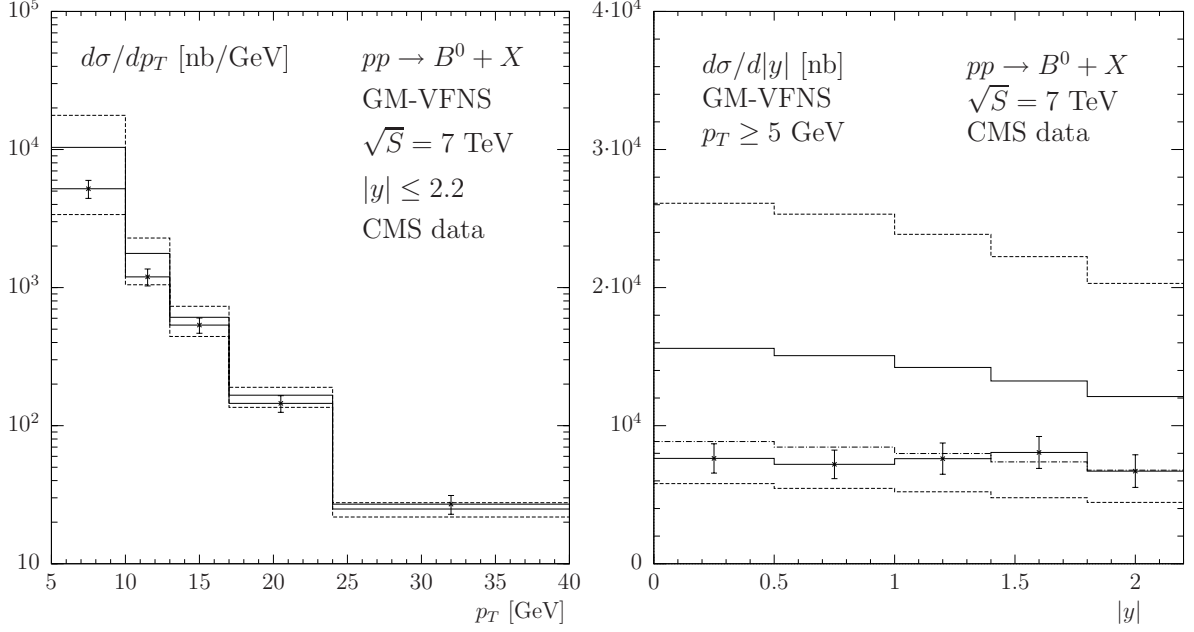


Figure 3:  $d\sigma/dp_T$  [nb/GeV] (left panel) and  $d\sigma/d|y|$  [nb] (right panel) for  $pp \rightarrow B^0 + X$  at NLO in the GM-VFN scheme compared with the CMS data [6]. The central values (solid lines) correspond to the choice  $\xi_R = \xi_F = 1$ . We also show the prediction for  $d\sigma/d|y|$  obtained with the choice  $\xi_R = 1$  and  $\xi_F = 0.7$  (dash-dotted line). The error bands (dashed lines) are obtained by varying  $\xi_R$  and  $\xi_F$  by factors of 2 up and down (maximum:  $\xi_R = 1$ ,  $\xi_F = 2$ ; minimum:  $\xi_R = 1$ ,  $\xi_F = 0.5$ ).

experimental results in the second column of this table and the default-scale results of Fig. 3 (left) in the third one. We see that the theoretical values of the cross sections in the five  $p_T$  bins agree with the experimental values quite well, within the errors. The total  $B^0$ -meson production cross section determined by CMS in the considered kinematic range is  $\sigma_{\text{tot}} = 33.2 \pm 4.3 \mu\text{b}$ . For the default choice of scales  $\xi_R = \xi_F = 1$ , we find  $\sigma_{\text{tot}} = 61.7 \mu\text{b}$ , while the result for  $\xi_R = 1$  and  $\xi_F = 0.7$  is  $35.0 \mu\text{b}$ , in very good agreement with the data. A similar comparison may be performed for  $pp \rightarrow B^+ X$ , with similar conclusions, as can be inferred from Fig. 2 (right panel), where we show the corresponding results for  $d\sigma/d|y|$ . The theoretical predictions are almost identical, since the FFs for  $b \rightarrow B^+$  and  $b \rightarrow B^0$  are taken to be the same and there is only a tiny difference due to the different upper ends of the  $p_T$  ranges.

As explained above, massless contributions, in particular the ones due to incoming  $b$  quarks, dominate the total cross section towards low  $p_T$  values. These contributions lead to an increase of  $d\sigma/dp_T$  in the limit  $p_T \rightarrow 0$  because the heavy-quark PDFs carry resummed logarithms, which are not fully cancelled by the subtraction terms in the GM-VFN approach, which are implemented at NLO, i.e. at fixed order only. This increase can be tamed by imposing the kinematic cut  $\hat{s} > 4m_b^2$  for the partonic center-of-mass energy

$p_T$ (in GeV)	Data [6]	$\xi_R = \xi_F = 1$	$\xi_R = 1, \xi_F = 0.7$	$\xi_a = 0.2$
5–10	$5200 \pm 770$	10356	5578	6327
10–13	$1196 \pm 168$	1769	1265	1016
13–17	$535 \pm 68$	610	481	401
17–24	$145 \pm 20$	166	141	124
24–40	$27 \pm 4$	25	22	21

Table 1: Predictions for the differential cross section  $d\sigma/dp_T$  [nb/GeV] of  $B^0$ -meson production with different renormalization and factorization scales compared with the CMS data [6], for which the statistical and systematic errors are added in quadrature. The values presented in the second and third columns are also displayed in Fig. 3 (left).

$\hat{s}$  also for the massless contributions. Furthermore, a judicious choice of the factorization scale, e.g.

$$\mu_F = \sqrt{m_b^2 + \xi_a p_T^2}, \quad (1)$$

with a parameter  $\xi_a < 1$ , can boost the transition  $\mu_F \rightarrow \mu_0 = m_b$  for  $p_T \rightarrow 0$ . This prescription creates a turn-over of the  $p_T$  distribution towards low  $p_T$  values and also allows us to obtain a reasonable description of the CDF data [4], which were taken at lower  $p_T$  values. The CMS data start at  $p_T = 5$  GeV, and a turn-over is not visible in  $d\sigma/dp_T$ . However, the ansatz of Eq. (1) leads to a reduction of the  $p_T$  distribution for small  $p_T$  values, i.e. to a significant change of  $d\sigma/dp_T$  in the first two  $p_T$  bins. The cross section values obtained for  $B^0$  mesons using the scale choice of Eq. (1) with  $\xi_a = 0.2$  are presented in the last column of Tab. 1. We find that this approach leads to a better description of the CMS data, which is, however, not as good as for the scale choice  $\xi_F = 0.7$  (fourth column of Tab. 1).

As a side remark, we note that the behavior towards small  $p_T$  values is not due to a shift in the average  $B$ -meson to  $b$ -quark momentum fraction. This may be observed by calculating the quantity

$$\langle z \rangle(p_T) = \frac{\int dz z d\sigma(p_T)}{\int dz d\sigma(p_T)}, \quad (2)$$

where  $z$  is the scaling variable of the FFs and it is understood that the integration is also done over the rapidity interval  $|y| \leq 2.4$  relevant for the CMS measurement [5]. We find a rather weak dependence on  $p_T$ . In fact,  $\langle z \rangle$  decreases from 0.770 at  $p_T = 5$  GeV to 0.749 at  $p_T = 30$  GeV, which means that, in our applications, the  $b \rightarrow B$  FF is always probed around its maximum (see Ref. [13]).

We now discuss the  $|y|$  distributions  $d\sigma/d|y|$  of  $B^+$  and  $B^0$  production shown in the right panels of Figs. 2 and 3, respectively. The bulk of these cross sections comes from the lowest  $p_T$  bin, where the theoretical uncertainties are largest, as is evident from Tab. 1. However, it is interesting to find out how much the shapes of these differential cross



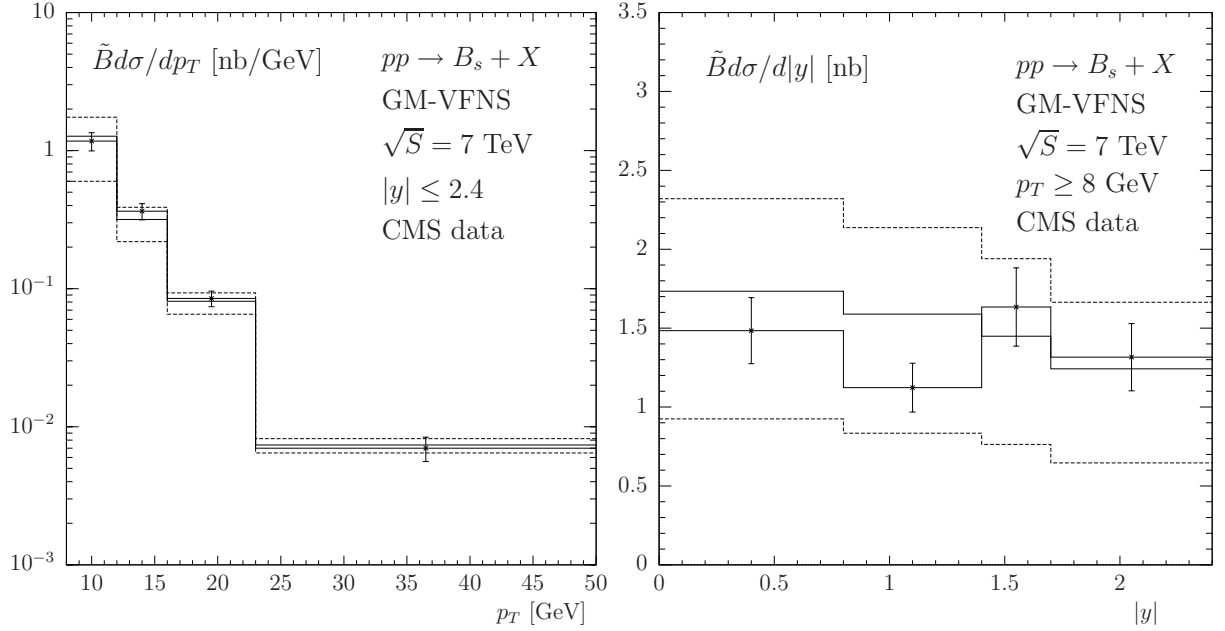


Figure 4:  $\tilde{B}d\sigma/dp_T$  [nb/GeV] (left panel) and  $\tilde{B}d\sigma/d|y|$  [nb] (right panel) for  $pp \rightarrow B_s + X$  at NLO in the GM-VFNS scheme compared with the CMS data [7]. The branching fraction of the decay  $B_s \rightarrow J/\psi\phi$  is assumed to be  $\tilde{B} = 1.3 \times 10^{-3}$  [22]. The central values (solid lines) correspond to the choice  $\xi_R = \xi_F = 1$ . The error bands (dashed lines) are obtained by varying  $\xi_R$  and  $\xi_F$  by factors of 2 up and down (maximum:  $\xi_R = 0.5$ ,  $\xi_F = 1$ ; minimum:  $\xi_R = 1$ ,  $\xi_F = 0.5$ ).

sections depend on the various scale choices. In order to get some idea about this, we include in the right panels of Figs. 2 and 3 as dot-dashed histograms also the predictions evaluated using the scale choice  $\xi_R = 1$  and  $\xi_F = 0.7$ , as in the fourth column in Tab. 1. They agree fairly well with the CMS data, while the default predictions ( $\xi_R = \xi_F = 1$ ), shown as solid histograms, significantly overshoot the CMS data as expected, but their shapes are still reasonable.

Finally, in Fig. 4, we present our predictions for the production of  $B_s$  mesons and compare them with the experimental data published by the CMS Collaboration in Ref. [7].  $d\sigma/dp_T$  was measured in four  $p_T$  bins between  $p_T = 8$  and 50 GeV and integrated over  $|y| \leq 2.4$ , and  $d\sigma/d|y|$  was measured in four  $|y|$  bins spanning this  $|y|$  range and integrated over the full  $p_T$  range considered. Both the experimental data and our theoretical predictions refer to the product of cross section times branching fraction  $\tilde{B}$  for  $B_s \rightarrow J/\psi\phi$ , for which we adopt the value  $1.3 \times 10^{-3}$  from Ref. [22]. In this case, we find better agreement between theory and experiment over the full  $p_T$  range, probably due to the fact that very low values of  $p_T$ , with  $p_T < 8$  GeV, are excluded from this analysis. The total cross section times branching fraction measured by CMS for  $8 \text{ GeV} \leq p_T \leq 50 \text{ GeV}$  and  $|y| \leq 2.4$  is  $6.9 \pm 0.8 \text{ nb}$ , while our calculation yields 7.2 nb.

## 4 Conclusions

In summary, we applied the GM-VFN scheme to obtain NLO predictions for the production of  $B$  mesons in  $pp$  collisions at the LHC. The comparison with experimental data from the CMS Collaboration at  $\sqrt{S} = 7$  TeV generally shows good agreement between theory and experiment, in particular at large  $p_T$  values. The agreement is particularly good for the case of  $B_s$ -meson production, where data are restricted to  $p_T$  values above 8 GeV. At low  $p_T$  values, we observe large scale uncertainties.

Future data collection at the LHC will allow us to extend the comparisons with theoretical predictions to much wider  $p_T$  ranges. If also the systematic uncertainties can be further reduced, we may expect that  $B$ -meson production will play an increasingly important role in constraining size and shape of both PDFs and FFs.

## References

- [1] C. Albajar *et al.* (UA1 Collaboration), Phys. Lett. B **213**, 405 (1988).
- [2] F. Abe *et al.* (CDF Collaboration), Phys. Rev. Lett. **75**, 1451 (1995) [arXiv:hep-ex/9503013]; D. E. Acosta *et al.* (CDF Collaboration), Phys. Rev. D **66**, 052005 (2002).
- [3] S. Abachi *et al.* (D0 Collaboration), Phys. Rev. Lett. **74**, 3548 (1995); B. Abbott *et al.* (D0 Collaboration), Phys. Rev. Lett. **84**, 5478 (2000) [hep-ex/9907029].
- [4] D. Acosta *et al.* (CDF Collaboration), Phys. Rev. D **71**, 032001 (2005) [arXiv:hep-ex/0412071]; A. Abulencia *et al.* (CDF Collaboration), Phys. Rev. D **75**, 012010 (2007) [hep-ex/0612015]; T. Aaltonen *et al.* (CDF Collaboration), Phys. Rev. D **79**, 092003 (2009) [arXiv:0903.2403 [hep-ex]].
- [5] V. Khachatryan *et al.* (CMS Collaboration), Phys. Rev. Lett. **106**, 112001 (2011) [arXiv:1101.0131 [hep-ex]].
- [6] S. Chatrchyan *et al.* (CMS Collaboration), Phys. Rev. Lett. **106**, 252001 (2011) [arXiv:1104.2892 [hep-ex]].
- [7] S. Chatrchyan *et al.* (CMS Collaboration), Phys. Rev. D **84**, 052008 (2011) [arXiv:1106.4048 [hep-ex]].
- [8] P. Nason, S. Dawson, and R.K. Ellis, Nucl. Phys. **B303**, 607 (1988); **B327**, 49 (1989); **B335**, 260(E) (1989); W. Beenakker, H. Kuijf, W.L. van Neerven, and J. Smith, Phys. Rev. D **40**, 54 (1989); W. Beenakker, W.L. van Neerven, R. Meng, G.A. Schuler, and J. Smith, Nucl. Phys. **B351**, 507 (1991); I. Bojak and M. Stratmann, Phys. Rev. D **67**, 034010 (2003) [arXiv:hep-ph/0112276].

- [9] M. Cacciari and M. Greco, Nucl. Phys. **B421**, 530 (1994) [arXiv:hep-ph/9311260]; B. A. Kniehl, M. Krämer, G. Kramer, and M. Spira, Phys. Lett. B **356**, 539 (1995) [arXiv:hep-ph/9505410]; M. Cacciari, M. Greco, B. A. Kniehl, M. Krämer, G. Kramer, and M. Spira, Nucl. Phys. **B466**, 173 (1996) [arXiv:hep-ph/9512246]; J. Binnewies, B. A. Kniehl, and G. Kramer, Z. Phys. C **76**, 677 (1997) [arXiv:hep-ph/9702408]; B. A. Kniehl, G. Kramer, and M. Spira, Z. Phys. C **76**, 689 (1997) [arXiv:hep-ph/9610267]; J. Binnewies, B. A. Kniehl, and G. Kramer, Phys. Rev. D **58**, 014014 (1998) [arXiv:hep-ph/9712482]; Phys. Rev. D **58**, 034016 (1998) [arXiv:hep-ph/9802231]; B. A. Kniehl and G. Kramer, Phys. Rev. D **60**, 014006 (1999) [arXiv:hep-ph/9901348]; B. A. Kniehl, in *Proceedings of the 14th Topical Conference on Hadron Collider Physics: Hadron Collider Physics 2002*, Karlsruhe, Germany, 2002, edited by M. Erdmann and Th. Müller (Springer, Berlin, 2003), p. 161 [arXiv:hep-ph/0211008]; B. A. Kniehl and G. Kramer, Phys. Rev. D **71**, 094013 (2005) [arXiv:hep-ph/0504058]; Phys. Rev. D **74**, 037502 (2006) [arXiv:hep-ph/0607306].
- [10] G. Kramer and H. Spiesberger, Eur. Phys. J. C **22**, 289 (2001) [arXiv:hep-ph/0109167]; Eur. Phys. J. C **28**, 495 (2003) [arXiv:hep-ph/0302081]; Eur. Phys. J. C **38**, 309 (2004) [arXiv:hep-ph/0311062]; B. A. Kniehl, G. Kramer, I. Schienbein, and H. Spiesberger, Phys. Rev. D **71**, 014018 (2005) [arXiv:hep-ph/0410289]; G. Kramer and H. Spiesberger, Phys. Lett. B **679**, 223 (2009) [arXiv:0906.2533 [hep-ph]].
- [11] B. A. Kniehl, G. Kramer, I. Schienbein, and H. Spiesberger, Phys. Rev. D **71**, 014018 (2005) [arXiv:hep-ph/0410289]; Eur. Phys. J. C **41**, 199 (2005) [arXiv:hep-ph/0502194]; AIP Conf. Proc. **792**, 867 (2005) [arXiv:hep-ph/0507068]; Phys. Rev. Lett. **96**, 012001 (2006) [arXiv:hep-ph/0508129]; Phys. Rev. D **79**, 094009 (2009) [arXiv:0901.4130 [hep-ph]].
- [12] T. Kneesch, B. A. Kniehl, G. Kramer, and I. Schienbein, Nucl. Phys. **B799**, 34 (2008) [arXiv:0712.0481 [hep-ph]].
- [13] B. A. Kniehl, G. Kramer, I. Schienbein, and H. Spiesberger, Phys. Rev. D **77**, 014011 (2008) [arXiv:0705.4392 [hep-ph]].
- [14] M. Cacciari, M. Greco, and P. Nason, JHEP **9805**, 007 (1998) [arXiv:hep-ph/9803400]; M. Cacciari and P. Nason, Phys. Rev. Lett. **89**, 122003 (2002) [arXiv:hep-ph/0204025]; M. Cacciari, P. Nason, and C. Oleari, JHEP **0604**, 006 (2006) [arXiv:hep-ph/0510032].
- [15] A. Heister *et al.* (ALEPH Collaboration), Phys. Lett. B **512**, 30 (2001) [arXiv:hep-ex/0106051].
- [16] G. Abbiendi *et al.* (OPAL Collaboration), Eur. Phys. J. C **29**, 463 (2003) [arXiv:hep-ex/0210031].

- [17] K. Abe *et al.* (SLD Collaboration), Phys. Rev. D **65**, 092006 (2002); **66**, 079905(E) (2002) [arXiv:hep-ex/0202031].
- [18] P. M. Nadolsky *et al.* (CTEQ Collaboration), Phys. Rev. D **78**, 013004 (2008) [arXiv:0802.0007 [hep-ph]].
- [19] J. Abdallah *et al.* (DELPHI Collaboration), Eur. Phys. J. C **71**, 1557 (2011) [arXiv:1102.4748 [hep-ex]].
- [20] C. Peterson, D. Schlatter, I. Schmitt, and P. M. Zerwas, Phys. Rev. D **27**, 105 (1983).
- [21] V. G. Kartvelishvili and A. K. Likhoded, Yad. Fiz. **42**, 1306 (1985) [Sov. J. Nucl. Phys. **42**, 823 (1985)].
- [22] K. Nakamura *et al.* (Particle Data Group), J. Phys. G **37**, 075021 (2010).